Published in final edited form as:
Cancer Res. 2017 November 1; 77(21): 5846–5859. doi:10.1158/0008-5472.CAN-16-3152.

Lysyl oxidase-like protein LOXL2 promotes lung metastasis of breast cancer

Fernando Salvador[#1,§], **Alberto Martin**[#1,3,&,§], **Celia López-Menéndez**[1], **Gema Moreno-Bueno**[1,2,3], **Vanesa Santos**[1,3], **Alberto Vázquez-Naharro**[1], **Patricia G. Santamaria**[1], **Saleta Morales**[1], **Pierre R. Dubus**[4,5], **Laura Muinelo-Romay**[3,6], **Rafael López-López**[3,6], **Jason C. Tung**[7], **Valerie M. Weaver**[7], **Francisco Portillo**[1,3], and **Amparo Cano**[1,3,&]

[1]Departamento de Bioquímica, UAM, Instituto de Investigaciones Biomédicas "Alberto Sols" CSIC-UAM, IdiPAZ, Arzobispo Morcillo, 4, 28029 Madrid, Spain

[2]Fundación MD Anderson International Madrid, Arturo Soria, 270, 28033 Madrid, Spain

[3]CIBERONC, Av Monforte de Lemos, 3-5, Pabellón 11, planta 0, 28029 Madrid, Spain

[4]Université de Bordeaux, INSERM UMR1053, 146 rue Léo Saignat, 33076 Bordeaux cedex, France

[5]CHU de Bordeaux, 12 rue Dubernat 33404 Talence cedex, France

[6]Translational Medical Oncology; Health Research Institute of Santiago (IDIS), SERGAS, Travesía da Choupana s/n, 15706 Santiago de Compostela, Spain

[7]Center for Bioengineering and Tissue regene ration; Department of Surgery, UCSF, 513 Parnasus Avenue, HSE 560, Box 0456, San Francisco, CA 94143-0456

[#] These authors contributed equally to this work.

Abstract

The lysyl oxidase-like protein LOXL2 has been suggested to contribute to tumor progression and metastasis, but *in vivo* evidence has been lacking. Here we provide functional evidence that LOXL2 is a key driver of breast cancer metastasis in two conditional transgenic mouse models of PyMT-induced breast cancer. LOXL2 ablation in mammary tumor cells dramatically decreased lung metastasis, whereas LOXL2 overexpression promoted metastatic tumor growth. LOXL2 depletion or overexpression in tumor cells does not affect extracellular matrix stiffness or organization in primary and metastatic tumors, implying a function for LOXL2 independent of its conventional role in extracellular matrix remodeling. In support of this likelihood, cellular and molecular analyses revealed an association of LOXL2 action with elevated levels of the EMT regulatory transcription factor Snail1 and expression of several cytokines that promote pre-metastatic niche formation. Taken together, our findings established a pathophysiological role and new function for LOXL2 in breast cancer metastasis.

[&]corresponding authors: Amparo Cano (acano@iib.uam.es), Alberto Martín (almmartin@isciii.es), Departamento de Bioquímica UAM, c/ Arzobispo Morcillo, 4, 28029 Madrid, Spain.
[§]Present address: FS. Oncology Program, Institute for Research in Biomedicine (IRB Barcelona) c/ Baldiri Reixac 10, 08028 Barcelona, Spain
AM. Instituto de Investigación de Enfermedades Raras (IIER), Instituto de Salud Carlos III, Carretera Majadahonda-Pozuelo km. 2. Majadahonda, 28220 Madrid, Spain

Europe PMC Funders Author Manuscripts

Keywords

LOXL2; breast cancer; metastasis; stiffness; Loxl2 genetic models

Introduction

LOXL2 (lysyl oxidase like-2) belongs to the lysyl oxidase (LOX) family of proteins composed of five members (LOX and four related enzymes, LOXL1-4) whose conventional function is to catalyze the crosslinking of extracellular matrix (ECM) components, mainly collagens and elastin (1–3). LOX family members thus play an essential role in tissue homeostasis contributing to ECM remodeling, but can also participate in diverse pathological conditions as organ fibrosis and cancer (4–7). Studies based on expression analyses in human tumors combined with functional assays in cell systems have implicated LOX and LOXL2 in progression and metastasis of several types of carcinomas (8–12). In particular, LOX and LOXL2 have been linked to metastasis of breast carcinoma (8, 12). One of the prominent actions of LOX in breast cancer metastasis is related to its ability to increase the ECM stiffness of primary tumors (6, 13) and promote collagen remodeling at distant organs to facilitate the recruitment of bone marrow derived cells (BMDC) to the pre-metastatic niche (14, 15). LOXL2 has also been associated with metastatic niche formation (16–18) but the underlying mechanisms are not yet fully understood. Initial studies suggested that LOXL2 action on tumorigenesis and metastasis could be similar to that of LOX, thus related to its potential ECM crosslinking activity (8, 18, 19). Nevertheless, subsequent studies demonstrated an unconventional action of intracellular LOXL2 in invasion and metastasis (12, 17, 20–22), including induction of epithelial to mesenchymal transition (EMT), Snail1 stabilization (a key EMT transcription factor), and activation of the UPR pathway (23, 24). LOXL2/Snail1-mediated repression of E-cadherin and other epithelial genes contributes to the dedifferentiated and metastatic phenotype of squamous cell carcinomas and basal breast carcinoma cells, respectively (12, 20). Of note, LOXL2-dependent transcriptional repression and EMT induction in cell culture systems does not require its catalytic activity (12, 17, 24, 25), indicating that, at least, part of LOXL2 unconventional actions in cancer may not depend on ECM remodeling. To date, the implication on LOXL2 in tumorigenesis and metastasis rely on cell model systems with overexpression or knockdown of LOXL2. However, the function of endogenous LOXL2 in *in vivo* tumor contexts and its relation/cooperation with other LOX/LOXL proteins has not been explored previously. We have recently reported the generation of constitutive *Loxl2* gain- and loss-of function genetic mouse models, characterized in the context of epidermal squamous cell carcinomas (22). In the present study we address the function of endogenous Loxl2 in breast cancer metastasis through the generation of two complementary mouse models that conditionally delete or overexpress *Loxl2* in the mammary gland of PyMT transgenic mouse model of breast cancer. *In vivo* targeting of Loxl2 in primary tumors from both models clearly revealed a direct correlation of Loxl2 with lung metastatic burden and pre-metastatic niche formation that, of note, was independent of both ECM stiffness and collagen organization of primary tumors and metastatic sites, as well as of Lox expression. Detailed cellular and molecular studies of PyMT tumors and derived cell lines from both complementary models indicated that the Loxl2 pro-metastatic action is mediated in tumor

Europe PMC Funders Author Manuscripts

cells by mechanisms that promote a dedifferentiated pro-invasive phenotype associated with increased Snail1 protein levels, and foster cytokine expression and the recruitment of immature myeloid cells to distant organs facilitating pre-metastatic niche formation. These results represent the first *in vivo* genetic study of a LOX family member in breast cancer, underlining the therapeutic value of LOXL2 as a druggable target.

Materials and Methods

Mice

MMTV-PyMT (PyMT) mice (FBV/n background) were purchased from The Jackson laboratory and *MMTV-Cre* (26) were obtained from the CNIO (Centro Nacional de Investigaciones Oncológicas) Transgenic Unit. Conditional Loxl2 deletion ($L2^{fl/fl}$) or overexpression ($R26^{STOPL2}$) mouse lines were recently described (22); presenting a mixed genetic background (50% FVB and 50% mix from C57BL/6, CD1 and 129v strains). PyMT mice harboring conditional Loxl2 deletion ($PyMT;L2^{\Delta/-}$) or overexpression ($PyMT;R26^{L2}$) in the mammary gland were generated by intercrossing $L2^{fl/fl}$ or $R26^{STOPL2}$ females with their corresponding $MMTV\text{-}PyMT^{+/T};MMTV\text{-}Cre^{+/T};Loxl2^{fl/-}$ and $MMTV\text{-}PyMT^{+/T};MMTV\text{-}Cre^{+/T};R26^{STOPL2}$ males. $PyMT^{+/T};L2^{fl/fl}$ *and* $PyMT^{+/T};R26^{STOPL2}$ mice lacking Cre expression ($Cre^{+/+}$) were used as littermate controls. All mouse studies were conducted in accordance with protocols approved by the Use Committee for Animal Care from the Universidad Autónoma de Madrid (UAM) (Ref# CEI-25-587) and the Comunidad de Madrid (PROEX 182/14).

Genotyping

Primers for conventional PCR genotyping are described in Supplementary Table S1.

RT-qPCR and semi-quantitative RT-PCR

Total RNA extraction from breast tumors, lungs and cells, cDNA synthesis and quantitative real-time PCR and semi-quantitative RT-PCR were performed as previously described (22). Each PCR reaction was carried out in triplicates from each tissue sample. Values were relativized to actin levels. Primer pairs are listed in Supplementary Table S2.

Flow cytometry

Lung, blood, and bone marrow samples were prepared for flow cytometry as previously described (17). Cell suspensions were incubated with CD11b and Gr1 fluorochrome-conjugated antibodies (Supplementary Table S3) diluted in PBS for 30-45 min at 4°C. Data were acquired on a CITOMICS FC-500 MPL cytometer (Beckman Coulter) and analyzed using MXP software.

Picrosirious red staining and quantification

Analyses were performed on 5 μm frozen or paraffin-embedded sections of primary or xenograft tissues, respectively, stained with 0.1% picrosirious red (Sigma) and counterstained with Weigert's hematoxylin to reveal fibrillar collagen. Frozen sections were imaged using an Olympus IX81 fluorescence microscope fitted with an analyzer (U-ANT)

and polarizer (U-POT, Olympus) oriented parallel and orthogonal to each other. Paraffin sections were digitalized with an Axioscan.Z1 equipment (Carl Zeiss) using polarized light and a x20 PlanApo objective (0.22 μm/pixel resolution) and analyzed with ZEN light (Carl Zeiss) and FIJI (NIH Image J) software. Images were quantified for pixel density threshold light intensity.

Atomic Force Microscopy (AFM)

Samples were prepared as previously described (27). Fresh mammary tumors were embedded in OCT within a disposable plastic base mold (Fisher) and were snap frozen via direct immersion into liquid nitrogen. Frozen tissue blocks were then cut in 50 μm sections using disposable low profile microtome blades (Leica, 819) on a cryostat (Leica, CM1900-3-1). Prior to AFM analysis, each section was thawed and OCT was removed by immersion in PBS at room temperature. Samples were maintained in proteinase inhibitor in PBS (protease inhibitor cocktail; Roche Diagnostics), with propidium iodide (SIGMA P4170, 20 μg/ml) during the AFM analysis. AFM measurements were obtained as previously described (28). Experiments were conducted using a MFP3D-BIO inverted optical AFM (Asylum Research) mounted on a Nikon TE200-U inverted fluorescence microscope. Silicon nitride cantilevers (spring constant=0.06 N/m) modified with a borosilicate glass spherical tip with a 5 μm diameter (Novascan Tech) were used for indentation. For each session, cantilevers were calibrated using the thermal oscillation method. AFM force maps were performed on 40 μm×40 μm fields. Each condition group contained a mammary gland from 4 different mice, with 2 sections from each mouse, and at least 5 maps generated per section. Data analyses were done using the Hertz model in Igor Pro (version 6.22A) and a Poisson's ratio of 0.5.

Primary cell cultures

PyMT tumor derived cells were obtained by mechanical dissociation of primary tumors followed by incubation with 0.1% collagenase for 30 min at 37°C and filtration through 70 μm sieves. After centrifugation cells were plated in HAM's F12 medium supplemented with 5% FBS, 2mM L-glutamine, 10 μg/ml insulin, 1 μg/ml hydrocortisone, 1% Penicillin-Streptomycin and fungizone, and cultured at 37°C under a 5% CO_2 atmosphere. Once stable cell lines were obtained, cultures were expanded and frozen within 2-3 passages. When needed, cells were thawed and transduced according to the protocol described below and experiments were performed 3-4 passages after adenoviral or retroviral infections (cells in use from 2015 to 2017). Primary and transduced cell lines were routinely tested for mycoplasma, the latest tests made on February 2017. Mice-derived cell lines were not authenticated.

Lentiviral and adenoviral infections

Human kidney 293T cells were transfected with 10 μg of packaging lentiviral constructs (PLP1, PLP2 and VsVg) plus 10 μg of GFP-Luciferase harboring vector (a gift from Dr. Santamaría, CNIO, Madrid). Cell supernatants containing infectious lentiviral particles were harvested 48–60 h post-transfection, pooled on ice and filtered (0.45 μm membrane). Viral infections of exponentially growing PyMT breast cancer cells were performed in a 5% CO_2 atmosphere with 5 ml of virus-containing culture supernatants plus 10 μg/ml polybrene.

After 5 h, 10 ml fresh medium was added, and medium was changed 24 h later. Cells were GFP-sorted 7 days after infection and then subjected to subsequent *in vitro* manipulations with GFP and Cre expressing adenovirus (a gift from Mariano Barbacid's Laboratory, CNIO, Madrid). Briefly, cells were incubated o.n. with medium containing purified adenovirus at a ratio of 15-20 infective particles/cell. Two consecutive infections were performed. For Snail1 ectopic expression, PyMT-Loxl2 deficient (Cre) and control (GFP) cell lines were transduced with control and Snail1 lentiviral particles (Origene) plus 8 μg/ml polybrene and selected with puromycin (1.5 μg/ml).

Tumourigenesis and metastasis assays

$0.25\text{-}0.5\times10^6$ cells in 100 μl of PBS were injected in the tail vein or mammary fat pad of Balb/C nude mice. Animals were imaged in an IVIS 100 chamber (Caliper Life Sciences) and data were recorded using Living Image software. Tumor dimensions were measured using a caliper. Metastatic quantification of spontaneous and experimental metastasis assays was performed 70 days later after tumor resection or intravenous injection.

Immunofluorescence

Snail1 detection was performed on 5 μm frozen sections of primary PyMT tumors, fixed in 4% paraformaldehyde in PBS-4% sucrose for 20 min, permeabilized with 0.2% Triton X-100, and incubated with anti-Snail1 antibodies (Cell Signaling Technology) o.n. at 4°C and appropriate secondary antibodies (Supplementary Table S3). Slides were mounted with Prolong (Invitrogen-Live Technologies). Images are single sections of a *z*-series acquired in a sequential mode using an inverted Zeiss LSM710 confocal microscope and 63x/1.40 Plan-Apochromatic objective. Pictures were processed with ZEN 2009 light Edition (Carl Zeiss MicroImaging) and Adobe CS3 Extended (Adobe Systems Inc.) software. Image analysis was performed with ImageJ free software.

Statistics

The Chi-square contingency test Yates correction, or Fisher's exact test, were used to determine the statistical significance of the percentage of *in* situ component and immunohistochemical E-cadherin and cytokeratin staining, using the SPSS 17.0 for statistical program (SPSS Inc.). For the rest of statistical analyses *p*-values were generated using Student's *t*-test (unpaired, 2-tailed); p-value<0.05 was considered significant. Error bars were calculated as standard error. Sample size and number of experiments are indicated in each of the Figures.

Results

Loxl2 promotes dedifferentiation and invasion of primary PyMT breast tumors

To examine the effect of endogenous *Loxl2* on mammary tumorigenesis and metastasis, two complementary mouse models carrying either mammary gland-specific deletion or overexpression of *Loxl2* within the *MMTV-PyMT* background were generated. The deletion model included the $PyMT^{+/T};MMTV\text{-}Cre^{+/T};L2^{fl/-}$ KO mice (hereafter referred as $PyMT;L2^{\Delta/-}$) and its respective $PyMT^{+/T};MMTV\text{-}Cre^{+/+};L2^{fl/fl}$ control mice (hereafter referred as $PyMT;L2^{fl/fl}$). The overexpression model encompassed the $PyMT^{+/T};MMTV\text{-}$

Cre$^{+/T}$;*R26*^{L2} mice carrying a GFP cassette (22) (hereafter referred as *PyMT;R26*^{L2}) and the *PyMT*$^{+/T}$;*MMTV-Cre*$^{+/+}$;*R26*^{STOPL2} control mice (hereafter referred as *PyMT;R26*^{STOPL2}). No significant differences were found in tumor incidence (data not shown) and size of the primary lesions developed by *PyMT;L2*$^{\Delta/-}$ KO or *PyMT;R26*^{L2} overexpressing mice regarding their respective control counterparts (Supplementary Fig. S1). A pronounced reduction of *Loxl2* mRNA levels in primary tumors from KO and a clear upregulation of *Loxl2* transcripts in tumors from overexpressing mice compared to their controls were confirmed (Supplementary Fig. S2A-B, left). Concerning the expression of other Lox members, only *Lox* was slightly upregulated in KO tumors and no significant changes were detected in the expression of the remaining *Loxl* genes in tumors from *Loxl2* KO or overexpressing mice compared to their respective controls (Fig. S2A-B, right). Importantly, *Loxl2* was found upregulated in PyMT tumors compared to normal mammary glands (Supplementary Fig. S3), as reported for LOXL2 protein in human breast tumors (12).

Histological analyses classified all PyMT tumors as adenocarcinomas regardless of Loxl2 expression (Fig. 1A and B); however, more than 70% of *PyMT;L2*$^{\Delta/-}$ KO tumors (13 out 18) contained areas of *in situ* carcinomas with defined non-invasive borders while this percentage decreased to 25% (3 out of 12) in tumors developed in *PyMT;L2*$^{fl/fl}$ control mice (p=0.0236) (Fig. 1A and C). *PyMT;R26*^{L2} overexpressing tumors, displaying GFP expression (22), showed almost no *in situ* component similar to their controls (Fig. 1B). These results suggest that Loxl2 KO tumors exhibit a more differentiated phenotype than their corresponding controls. RT-qPCR analyses of luminal differentiation markers in adenocarcinomas from 14 week-old mice confirmed significant upregulation of *Csnb*, *Car3*, *Car6*, *Fabp4* and *Wap* genes in *PyMT;L2*$^{\Delta/-}$ KO tumors relative to *PyMT;L2*$^{fl/fl}$ adenocarcinomas (Fig. 1D). Similar analyses in *PyMT;R26*^{L2} overexpression tumors revealed decreased *Car3* and *Cdh1 mRNA* levels compared to *PyMT;R26*^{STOPL2} control tumors (Fig. 1E). Decreased E-cadherin expression was confirmed by immunohistochemistry in *PyMT;R26*^{L2} overexpressing lesions (n=15) showing reduced or delocalized E-cadherin stain at distinct tumor areas in 70% of tumors (p= 0.038) compared to their controls (n=12) and *PyMT-Loxl2* KO tumors that exhibited homogeneous E-cadherin membrane expression (Fig. 1F and Supplementary Table S4).

Together, these data suggest that Loxl2 overexpression induces a less differentiated and more invasive phenotype corroborating LOXL2 association with invasion and poor prognosis in human breast tumors (12).

Loxl2 is required for lung metastasis of PyMT breast tumors

Next, we analyzed the influence of Loxl2 depletion and overexpression in the PyMT tumors on pulmonary metastasis. Examination of lung metastatic lesions from 16 week-old tumor harboring mice revealed a clear reduction in metastatic burden in *PyMT;L2*$^{\Delta/-}$ KO mice compared to *PyMT;L2*$^{fl/fl}$ control animals (Fig. 2A). Metastatic incidence was 75% lower in the absence of *Loxl2* and a clear reduction in the number of larger metastatic foci was also evident in the lungs from KO mice compared to control animals (Fig. 2B). Remarkably, *PyMT;R26*^{L2} overexpressing mice showed the opposite phenotype with significantly higher pulmonary metastatic load in both number and size of metastatic lesions, also GFP labeled,

as compared to their control counterparts (Fig. 2C and D). The differences in metastatic foci between the control cohorts of both models are likely due to the slightly different genetic background of both models (29, 30). Similar analyses in 14 week-old mice revealed the absence of metastasis in *PyMT;R26*^{L2} overexpression mice and their controls whereas only a few micrometastatic foci were detected in one *PyMT-Loxl2* KO and three control mice (Supplementary Fig. S4). These results strongly support the direct involvement of Loxl2 in metastasis dissemination and outgrowth *in vivo*.

As an additional parameter of the metastatic spread potential of the tumors developed by both mice models, the number of circulating tumor cells (CTCs) was determined. Analysis of CTCs demonstrated a remarkable reduction in CTCs content in peripheral blood from *PyMT;L2*$^{\Delta/-}$ KO mice relative to controls and a slight increase in the *PyMT;R26*^{L2} overexpressing mice compared to the corresponding controls (Supplementary Fig. S5).

The collective results obtained in both complementary *Loxl2* mouse models clearly indicate that Loxl2 expression directly correlates with breast tumor aggressiveness, epithelial dedifferentiation and lung metastatic burden. Interestingly, Loxl2 pro-metastatic action in both model systems appears to be independent of the expression of Lox and other Loxl members.

Loxl2 does not affect biomechanical properties of the ECM in PyMT tumors

The metastatic action of LOX has been associated with promotion of ECM stiffness in different cell tumor systems (6, 13). Therefore, we next asked whether LOXL2 modifies the ECM stiffness in PyMT tumors. We thus examined the biomechanical ECM properties in primary tumors from *PyMT;L2*$^{\Delta/-}$ KO and *PyMT;R26*^{L2} overexpressing mice and corresponding controls. Neither abrogation nor overexpression of *Loxl2* in breast tumor cells promoted any significant change in the collagen fibrils content in the surrounding neoplastic stroma, determined by the birefringence intensity of picrosirious red-stained tumors (Fig. 3A and B). Accordingly, atomic force microscopy indentation computed similar collagen ECM stiffness in all PyMT tumors irrespective of their *Loxl2* status (Fig. 3C and D).

Considering that ECM remodeling has also been proposed as one of the initial events mediated by LOX in the pre-metastatic niche formation (15), we then analyzed the collagen organization within the local microenvironment of the lung stroma in early metastatic lesions from *PyMT;L*$^{\Delta/-}$ KO and *PyMT;R26*^{L2} overexpressing mice. Analogous to primary lesions, no significant correlation between Loxl2 levels and fibrillar collagen deposition and organization in lungs was detected (Supplementary Fig. S6A-B), excluding the implication of Loxl2 in ECM remodeling at early metastatic sites.

These data indicate that Loxl2 promotion of PyMT metastasis is independent of its potential ability to modify ECM stiffness and collagen organization of primary tumors or distant target microenvironment.

Loxl2 facilitates metastatic niche formation by driving the recruitment of CD11b+/Gr1+ cells and enhancing cytokine expression

To understand the molecular mechanisms responsible for the critical role of tumor Loxl2 in lung metastasis, we next investigated the *in vivo* relevance of Loxl2 in metastatic niche formation at early metastatic stages. Given the role of the myeloid progenitor CD11b+/Gr1+ cell population in the formation of the pre-metastatic niche (31, 32), we analyzed the involvement of tumor Loxl2 in the dynamics of this particular BMDC subset in bone marrow, blood, and lung samples from KO animals and control littermates at an early metastatic stage (14 week-old), when only few micrometastasis were detected in PyMT-KO and control mice (Supplementary Fig. S4). A striking expansion of CD11b+/Gr1+ cells was observed in each of the examined tissues from tumor-harboring mice compared to tumor-free wild-type animals (Fig. 4A and B). Importantly, $PyMT;L2^{\Delta/-}$ KO mice exhibited a significantly reduced CD11b+/Gr1+ cell population in the three tissue compartments compared to their corresponding control mice (Fig. 4A). Noticeably, analyses of CD11b+/Gr1+ cells in samples from $PyMT;R26^{L2}$ overexpressing mice revealed the opposite situation: an enrichment of this population in each of the examined tissues relative to control $PyMT;R26^{STOPL2}$ mice (Fig. 4B). Similar analyses in 12 week-old animals revealed low BMDC mobilization and no differences between genotypes (data not shown). Altogether, these data support a contribution of Loxl2 to myeloid cell mobilization and recruitment, thereby associating Loxl2 expression to pre-metastatic niche formation.

Another feature impacting on the pre-metastatic niche formation is the production by both primary tumors and target organs of different cytokines and growth factors (33–35). As such, we analyzed their expression in primary mammary tumors and early metastatic lungs recovered from both mice models. *Loxl2* deficiency in the mammary gland induced a strong downregulation in the expression of *S100A8*, *S100A9* and *GM-CSF* chemokines in both breast tumors and lungs compared to control counterparts (Fig. 4C). Conversely, *Loxl2* overexpression lead to significantly increased *S100A8 and S100A9* expression in tumors and lungs relative to control mice and no changes in *GM-CSF* levels (Fig. 4D). Levels of *TNF-α* and *VEGF* also decreased in tumors of KO mice and remained invariant in tumors and lungs from Loxl2 overexpressing mice compared to their respective controls (Fig. 4E and data not shown). Conversely, *tenascin-C* and *fibronectin* expression was increased in lungs from $PyMT;R26^{L2}$ overexpressing mice and remained unchanged in lungs from $PyMT;L2^{\Delta/-}$ KO mice compared to controls (Fig. 4F and Supplementary Fig. S7A-B).

Collectively, these data demonstrate that Loxl2 is actively participating *in vivo* in early metastatic stages of breast tumors by controlling the expression of several cytokines and secreted factors and favoring the mobilization and recruitment of myeloid CD11+/Gr1+ cells to lung metastatic sites.

Loxl2 promotes mammary metastatic spread in a cell autonomous fashion

To further investigate the action of endogenous tumor Loxl2 on tumorigesis and metastasis we derived primary PyMT cell lines in order to manipulate Loxl2 levels in pre-existing breast carcinoma cells *in vitro* so as to avoid potential confounding effects arising as a consequence of MMTV-Cre expression targeting cells outside the mammary gland

compartment (36). Three different primary breast tumor cell lines derived from *PyMT;L2*$^{fl/fl}$ mice were obtained and manipulated *in vitro* by lentiviral introduction of a *Luc* reporter gene to allow bioluminescence detection. These cells were subsequently infected with adenovirus encoding control GFP or Cre recombinase and *Loxl2* excision was confirmed at the mRNA level (Fig. 5A). Then, PyMT-control and PyMT-*Loxl2* deleted cells were injected in the mammary fat pad of nude mice and tumor growth was monitored. Both control and Loxl2 deficient cells produced neoplastic lesions with similar kinetics (Fig. 5B, left), recapitulating the *in vivo* phenotype. The influence of *Loxl2* removal on metastatic tumor burden was then analyzed in spontaneous metastasis assays after surgical resection of the primary tumors. A clear decrease in metastatic load was detected in mice injected with *Loxl2* depleted cells compared to control cells (Fig. 5B, right). Tail vein injection assays also revealed that ablation of *Loxl2* resulted in abrogation of lung colonization by PyMT cells up to 70 days post-injection (Fig. 5C, right). Lung inspection at necropsy revealed macrometastasis in most samples derived from mice injected with control cells, while mice inoculated with *Loxl2* deleted cells were devoid of metastatic foci (Fig. 5C, left).

A similar strategy was followed with three different primary breast tumor cell lines derived from *PyMT*;*R26*^{STOPL2} mice (Supplementary Fig. S8A). No significant differences in tumor growth rate were detected between PyMT-control and PyMT-*R26*^{L2} cells (Supplementary Fig. S8B, upper); however, increased number of lung metastatic foci was scored in mice orthotopically injected with Loxl2 overexpressing cells compared to their controls (Supplementary Fig. S8B, bottom) reinforcing the positive pro-metastastic action of Loxl2. Of note, the number of metastatic foci generated by PyMT-control cells was much lower in the spontaneous metastasis setting than in control genetic models (compare Figs. 5B and S8B with Fig 2B and D), as observed in other PyMT models (37, 38).

The contribution of Loxl2 to ECM remodeling in the PyMT xenografts generated from both models was also studied with no observable differences detected with regard to the collagen fibril content between the analyzed xenografts and their corresponding controls (Supplementary Fig. S9A-B). Collectively, these data support the conclusion that Loxl2 is required for metastatic seeding and/or colonization even in the absence of the primary tumor, likely involving the existence of cell autonomous mechanisms.

Loxl2 mediates invasiveness of PyMT cells modulating Snail1 expression levels

To determine the nature of cell autonomous processes orchestrated by Loxl2, we performed a functional and molecular characterization of PyMT cells with deregulated Loxl2 expression. In agreement with the *in vivo* tumorigenic behavior, PyMT-derived cells showed similar proliferation rates and cell cycle distribution regardless of Loxl2 status (data not shown). Noticeably, depletion of Loxl2 resulted in decreased invasiveness of PyMT cells through matrigel coated membranes compared to controls (Fig. 6A), mimicking the poor invasive behavior of primary *PyMT;L2*$^{\Delta/-}$ KO tumors (Fig. 1A and C) while PyMT-Loxl2 overexpressing cells exhibited a reverse invasive behavior (Fig. 6A). To explore the molecular mechanism underlying the Loxl2 pro-invasive phenotype, we analyzed the expression levels of different EMT markers and cell signaling pathways, previously shown to link Loxl2 to migratory/invasive traits (12, 17, 20, 39). No consistent changes were

detected in activated FAK/c-Src pathway regardless Loxl2 expression (Fig. 6B). Regarding EMT markers, Snail1 levels were consistently correlated with Loxl2 status, being downregulated in PyMT-Loxl2 KO and increased in Loxl2 overexpressing cells while no changes were detected in other EMT factors, like E47 (Fig 6B and data not shown). No changes in *Snail1* mRNA level were detected in PyMT cells irrespective of their Loxl2 status (Fig. 6C) suggesting that Loxl2 could promote Snail1 stability in PyMT cells, as previously reported in other cell systems (23, 40, 41). Importantly, nuclear Snail1 staining was significantly decreased in primary *PyMT;L2*$^{\Delta/-}$ KO tumors compared to their controls (Fig. 6D and E), strongly supporting the Loxl2-Snail1 link *in vivo*. To further confirm this molecular connection, Snail1 was re-expressed in PyMT-Loxl2 deficient cells (Fig. 7A) and the effect on invasion analyzed. Indeed, Snail1 overexpression in PyMT-Loxl2 deficient cells fully restored their invasive abilities up to levels similar to control Loxl2 proficient cells (Fig. 7B). To analyze the Loxl2-dependent invasive pattern of PyMT cells, the expression of CK14, involved in leading collective invasion of breast cancer cells (42), was studied in xenograft tumors. Most xenografts from PyMT-Loxl2 overexpressing cells (8/10) exhibited high CK14 expression at invasive tumor areas compared to their controls showing absence or reduced CK14 expression at invasive borders (7/9) (Supplementary Fig. S10A-B), suggesting that Loxl2 overexpression promotes collective invasiveness.

These data provide an *in vivo* support to the Loxl2-Snail1 axis as one mechanisms facilitating invasion of PyMT tumors and their derived cell lines.

Discussion

LOXL2 has been associated with breast cancer metastasis in human samples (12) and its functional implication as a pro-metastatic molecule has been proposed in cell and xenograft-based model studies (8, 12, 17–19). However, the role of endogenous LOXL2 *in vivo* has not been previously investigated. The critical implication of LOXL2 in breast cancer metastasis is herein strengthened in two complementary genetic mouse models carrying conditional mammary gland-specific deletion or overexpression of *Loxl2* in the *PyMT* breast cancer model. The MMTV-*PyMT* background recapitulates many processes found in human breast cancer progression generating highly aggressive tumors that metastasize to the lung within 3-4 months (43, 44). Remarkably, the two complementary *PyMT-Loxl2* transgenic models now described provide compelling evidence for the *in vivo* pro-metastatic action of tumor LOXL2 in breast cancer. Thus, *Loxl2* deletion in primary tumors resulted in a dramatic decrease of lung metastatic burden while its overexpression produced the opposite effect. This behavior is paralleled by the alteration of cell differentiation and invasiveness of primary tumors supporting Loxl2 implication in the regulation of both tumor properties.

The present PyMT-*Loxl2* models also evidence the involvement of Loxl2 in the generation of the pre-metastatic niche. Noticeably, a direct correlation between Loxl2 levels and CD11b +/Gr1+ mobilization and recruitment to early metastatic lungs was detected in the *Loxl2* KO and overexpressing mouse models, strongly supporting the *in vivo* participation of Loxl2 in this critical step of metastasis initiation either directly or as a consequence of increased CTCs. Further, Loxl2 within PyMT tumors regulates the expression of several cytokines as well as a subset of ECM components required for the generation of a permissive pre-

metastatic microenvironment (33, 34, 45, 46). Among them, S100A8 and S100A9, chemokines involved in the recruitment of CD11b+/Gr1+ cells (33, 35, 47), are profoundly affected by Loxl2 status, being both chemokines strongly downregulated in primary tumors and early metastatic lung sites of *Loxl2* KO mice and upregulated at both sites in *Loxl2* overexpressing mice. Other secreted factors like GM-CSF, TNF-α and VEGF, involved in S100A8/S100A9 expression and BMDC expansion (32, 48), are also downregulated in tumors and/or early metastatic lungs from KO mice. In addition, fibronectin and tenascin-C, required for promoting a selective microenvironment for BMDC recruitment at pre-metastatic sites (33, 45, 46), are upregulated in early metastatic lungs of *Loxl2* overexpressing mice. Importantly, our previous studies demonstrated a Loxl2-mediated transcriptional regulation of TNF-α and GM-CSF, thereby providing functional evidence for the requirement of GM-CSF and fibronectin for the completion of Loxl2 pro-metastatic action in syngeneic models (17). Collectively, the present data demonstrate the positive contribution of Loxl2 to early metastasis *in vivo* by regulating the expression of soluble cytokines and ECM components required for CD11b+/Gr1+ recruitment to target organs.

Remarkably, our present study of genetic *PyMT-Loxl2* models indicate that neither ECM stiffness nor collagen organization in primary tumors, early metastatic lungs or tumor xenografts are affected by Loxl2 deletion or overexpression, strongly supporting the conclusion that LOXL2 pro-metastatic action is intrinsic to breast tumor cells and independent of its potential extracellular action on the ECM. These results contrast with the reported LOX pro-metastatic functions in xenograft breast cancer models that rely on the ability of LOX to increase the ECM stiffness of the primary tumors (6, 13) and promote collagen-IV crosslinking at pre-metastatic sites (15). They also contrast with previous data implying that LOXL2-mediated collagen organization in xenografts influences tumor growth, invasive properties and metastatic colonization (16, 18, 49). These discrepancies are likely explained by the different experimental settings used among the diverse studies. However, it is also noteworthy that the Loxl2 pro-metastatic action in PyMT breast tumors is not compensated by other Lox family members as their expression was not significantly modified by *Loxl2* depletion or overexpression, except for *Lox* that was slightly upregulated in *PyMT-Loxl2* deficient tumors. A similar situation was also found in syngeneic mouse models were Loxl2 knockdown almost abolished lung metastasis independently of Lox and other Loxl members (17). Together, these data indicate specific and non-redundant functions for Lox and Loxl2 in metastasis and support a key action of Loxl2 in promoting breast cancer metastasis in *in vivo* contexts.

Noticeably, PyMT-derived cells with Loxl2 deletion or overexpression recapitulate the Loxl2 pro-metastatic role exposed *in vivo* in both PyMT transgenic models, further supporting a major action of intra-tumor Loxl2 over a potential stromal cell contribution. PyMT-derived cells from both *Loxl2* genetic models show an invasive behavior directly related to Loxl2 levels. Besides being in agreement with the pro-invasive LOXL2 behavior in breast cancer cells (8, 12, 17, 50) our present data extend to the *in vivo* phenotype. The altered invasiveness of *PyMT-Loxl2* deleted and overexpressing cells is in full agreement with the increased *in situ* component exhibited by primary tumors of *PyMT-Loxl2* KO mice and with the partial loss of E-cadherin expression found in tumors of *PyMT-Loxl2* overexpressing mice. Among the different intracellular Loxl2 targets able to mediate the pro-invasive

phenotype, we identified Snail1 as one strong candidate. In fact, nuclear Snail1 staining and total Snail1 protein levels are directly related to Loxl2 levels in primary PyMT tumors and invasiveness of PyMT-derived cells, respectively, supporting previous evidence of LOXL2-dependent Snail1 post-translational stabilization (23). Interestingly, transient Snail1 expression has been elegantly shown to be required for efficient breast cancer metastasis (51). Thus, our present data provide a molecular mechanism to facilitate the Loxl2-proinvasive and pro-metastatic function involving the participation of Snail1, although the *in vivo* importance of Snail1 remains to be determined. The CK14 pattern detected in xenografts from PyMT-Loxl2 overexpressing cells supports a collective migration mechanism, as recently reported for other PyMT-derived cells (42).

Loxl2 negatively regulates the differentiation status of PyMT tumors, as evidenced from the differential expression of luminal differentiation markers in primary tumors from the two complementary *PyMT-Loxl2* genetic models. This fact, together with the proposed Loxl2 involvement in EMT and Snail1 stabilization (23, 40, 41) and in tumor cell stemness (52), provides additional Loxl2-dependent mechanisms, not necessarily linked to its enzymatic activity (25), to control tumor progression. The ability of LOXL2 to negatively regulate tumor differentiation *in vivo* has been demonstrated in squamous cell carcinoma (22).

The present data also suggest that LOXL2 could temporarily precede and complement LOX function in the metastatic cascade of *in vivo* breast tumors; thus, LOXL2 promotion of stemness, invasion and dedifferentiation of breast cancer cells could pave the way for the extracellular LOX action on ECM stiffness at primary tumors and metastatic niche of target organs. Recent studies simultaneously targeting LOX and LOXL2 with small molecule inhibitors (53) lend support to this hypothesis. Further studies, including double conditional *Loxl2/Lox* KO mice, are required to clarify the relationship between these LOX members in the metastatic process.

In summary, our data reveal a critical action of breast tumor Loxl2 in promoting lung metastasis *in vivo* by enhancing dedifferentiation and tumor invasion as well as facilitating the formation of the pre-metastatic niche, independently of ECM stiffness or collagen organization at primary tumors or metastatic sites. Consequently, therapeutic strategies targeting LOXL2 should be aimed at blocking intra-tumor LOXL2, for which the *Loxl2* genetic models here described provide valuable preclinical models.

Supplementary Material

Refer to Web version on PubMed Central for supplementary material.

Acknowledgments

We thank our colleagues for providing reagents, and members of Amparo Cano's lab for their helpful suggestions, Raquel Arocha for help with mice colonies maintenance, Laura Molero (SIdI-UAM) for help with flow cytometry and Dr. Bruno Sainz (UAM) for advice in Sirius red analyses.

Financial Support

This work has been supported by grants from the Spanish Ministry of Economy and Innovation SAF2010-21143 (A. Cano, F. Portillo), SAF2013-44739-R (A. Cano, P.G. Santamaría, F. Portillo), SAF2016-76504-R (A. Cano, C.

López-Menéndez, P.G. Santamaría, F. Portillo) and CONSOLIDER-INGENIO 2010 CSD2007-00017 (A. Cano), the Spanish Instituto de Salud Carlos III [(RETIC-RD12/0036/0007 (A. Cano, G. Moreno-Bueno, P.G. Santamaria, F. Portillo) and CIBERONC (A. Cano, G. Moreno-Bueno, F. Portillo, R. López-López, L. Muinelo-Romay), PI13/00132 (G. Moreno-Bueno)] (all partly supported by FEDER funds); the AICR (12–1057) (A. Cano, A. Martin, P.G. Santamaría), WWCR (16–0295) (A. Cano, F. Portillo, P.G. Santamaría), Comunidad de Madrid (S2010/BMD-2303) (A. Cano, G. Moreno-Bueno), AECC-2011 (G. Moreno-Bueno) and TV3-Telemarató 2013 (G. Moreno-Bueno). A. Martin, F. Salvador, and A. Vázquez-Naharro were funded by the JAE-CSIC program, S2010/BMD-2303, SAF2013-44739-R and AICR grants; P.G. Santamaría by a contract from Fundación AECC (Spain) and, presently, by WWCR (16–0295) grant; V. Santos by CSD2007-00017, AICR (12–1057) and SAF2013-44739-R grants, and S. Morales by RETIC-RD12/0036/0007 grant.

Abbreviations

AFM	atomic force microscopy
BMDC	bone marrow derived cells
CTCs	circulating tumor cells
ECM	extracellular matrix
EMT	Epithelial-to-mesenchymal transition
GFP	green fluorescent protein
GM-CSF	granulocyte macrophage-colony stimulating factor
H&E	hematoxylin and eosin
KO	knock-out
LOX	lysyl oxidase
LOXL2	lysyl oxidase-like 2
MMTV	mouse mammary tumor virus
PyMT	polyoma middle T
R26	Rosa 26 locus
TNF-α	tumor necrosis factor α
VEGF	vascular endothelial growth factor

References

1. Lucero HA, Kagan HM. Lysyl oxidase: an oxidative enzyme and effector of cell function. Cell Mol Life Sci. 2006; 63:2304–16. [PubMed: 16909208]
2. Kim YM, Kim EC, Kim Y. The human lysyl oxidase-like 2 protein functions as an amine oxidase toward collagen and elastin. Mol Biol Rep. 2011; 38:145–9. [PubMed: 20306300]
3. Moon HJ, Finney J, Ronnebaum T, Mure M. Human lysyl oxidase-like 2. Bioorg Chem. 2014; 57:231–41. [PubMed: 25146937]
4. Barker HE, Cox TR, Erler JT. The rationale for targeting the LOX family in cancer. Nat Rev Cancer. 2012; 12:540–52. [PubMed: 22810810]
5. Cano A, Santamaria PG, Moreno-Bueno G. LOXL2 in epithelial cell plasticity and tumor progression. Future Oncol. 2012; 8:1095–108. [PubMed: 23030485]

6. Cox TR, Bird D, Baker AM, Barker HE, Ho MW, Lang G, et al. LOX-mediated collagen crosslinking is responsible for fibrosis-enhanced metastasis. Cancer Res. 2013; 73:1721–32. [PubMed: 23345161]
7. Trackman PC. Lysyl oxidase isoforms and potential therapeutic opportunities for fibrosis and cancer. Expert Opin Ther Targets. 2016; 20:935–45. [PubMed: 26848785]
8. Barker HE, Chang J, Cox TR, Lang G, Bird D, Nicolau M, et al. LOXL2-mediated matrix remodeling in metastasis and mammary gland involution. Cancer Res. 2011; 71:1561–72. [PubMed: 21233336]
9. Cox TR, Erler JT. Lysyl oxisades in colorectal cancer. Am J Physiol Gastrointest Liver Physiol. 2013; 305:G659–66. [PubMed: 24008360]
10. Cox TR, Gartland A, Erler JT. Lysyl oxidase, a targetable secreted molecule involved in cancer metastasis. Cancer Res. 2016; 76:188–92. [PubMed: 26732355]
11. Cox TR, Rumney RM, Schoof EM, Perryman L, Høye AM, Agrawal A, et al. The hypoxic cancer secretome induces pre-metastatic bone lesions through lysyl oxidase. Nature. 2015; 522:106–10. [PubMed: 26017313]
12. Moreno-Bueno G, Salvador F, Martín A, Floristán A, Cuevas EP, Santos V, et al. Lysyl oxidase-like 2 (LOXL2), a new regulator of cell polarity required for metastatic dissemination of basal-like breast carcinomas. EMBO Mol Med. 2011; 3:528–44. [PubMed: 21732535]
13. Levental KR, Yu H, Kass L, Lakins JN, Egeblad M, Erler JT, et al. Matrix crosslinking forces tumor progression by enhancing integrin signaling. Cell. 2009; 139:891–906. [PubMed: 19931152]
14. Erler JT, Bennewith KL, Nicolau M, Dornhöfer N, Kong C, Le QT, et al. Lysyl oxidase is essential for hypoxia-induced metastasis. Nature. 2006; 440:1222–26. [PubMed: 16642001]
15. Erler JT, Bennewith KL, Cox TR, Lang G, Bird D, Koong A, et al. Hypoxia-induced lysyl oxidase is a critical mediator of bone marrow cell recruitment to form the premetastatic niche. Cancer Cell. 2009; 15:35–44. [PubMed: 19111879]
16. Wong CC, Gilkes DM, Zhang H, Chen J, Wei H, Chaturvedi P, et al. Hypoxia-inducible factor 1 is a master regulator of breast cancer metastatic niche formation. Proc Natl Acad Sci USA. 2011; 108:16369–74. [PubMed: 21911388]
17. Canesin G, Cuevas EP, Santos V, López-Menéndez C, Moreno-Bueno G, Huang Y, et al. Lysyl oxidase-like 2 (LOXL2) and E47 EMT factor: novel partners in E-cadherin repression and early metastasis colonization. Oncogene. 2015; 34:951–64. [PubMed: 24632622]
18. Wong CC, Tse AP, Huang YP, Zhu YT, Chiu DK, Lai RK, et al. Lysyl oxidase-like 2 is critical to tumor microenvironment and metastatic niche formation in hepatocellular carcinoma. Hepatology. 2014; 60:1645–58. [PubMed: 25048396]
19. Barry-Hamilton V, Spangler R, Marshall D, McCauley S, Rodriguez HM, Oyasu M, et al. Allosteric inhibition of lysyl oxidase-like-2 impedes the development of a pathologic microenvironment. Nat Med. 2010; 16:1009–17. [PubMed: 20818376]
20. Peinado H, Moreno-Bueno G, Hardisson D, Pérez-Gómez E, Santos V, Mendiola M, et al. Lysyl oxidase-like 2 as a new poor prognosis marker of squamous cell carcinomas. Cancer Res. 2008; 68:4541–50. [PubMed: 18559498]
21. Millanes-Romero A, Herranz N, Perrera V, Iturbide A, Loubat-Casanovas J, Gil J, et al. Regulation of heterochromatin transcription by Snail1/LOXL2 during epithelial-to-mesenchymal transition. Mol Cell. 2013; 52:746–57. [PubMed: 24239292]
22. Martin A, Salvador F, Moreno-Bueno G, Floristán A, Ruiz-Herguido C, Cuevas EP, et al. Lysyl oxidase-like 2 represses Notch1 expression in the skin to promote squamous cell carcinoma progression. EMBO J. 2015; 34:1090–109. [PubMed: 25759215]
23. Peinado H, Del Carmen Iglesias-de la Cruz M, Olmeda D, Csiszar K, Fong KS, Vega S, et al. A molecular role for lysyl oxidase-like 2 enzyme in snail regulation and tumor progression. EMBO J. 2005; 24:3446–58. [PubMed: 16096638]
24. Cuevas EP, Eraso P, Mazón MJ, Santos V, Moreno-Bueno G, Cano A, et al. Loxl2 drives epithelial-mesenchymal transition via activation of IRE1-XBP1 signalling pathway. Sci Rep. 2017; 7:44988. [PubMed: 28332555]

25. Cuevas EP, Moreno-Bueno G, Canesin G, Santos V, Portillo F, Cano A. LOXL2 catalytically inactive mutants mediate epithelial-to-mesenchymal transition. Open Biol. 2014; 15:129–37.
26. Andrechek ER, Hardy WR, Siegel PM, Rudnicki MA, Cardiff RD, Muller WJ. Amplification of the neu/erbB-2 oncogene in a mouse model of mammary tumorigenesis. Proc Natl Acad Sci U S A. 2000; 97:3444–9. [PubMed: 10716706]
27. Pickup MW, Laklai H, Acerbi I, Owens P, Gorska AE, Chytil A, et al. Stromally derived Lysyl oxidase promotes metastasis of transforming growth factor-β–deficient mouse mammary carcinomas. Cancer Res. 2013; 73:5336–46. [PubMed: 23856251]
28. Lopez JI, Kang I, You WK, McDonald DM, Weaver VM. In situ force mapping of mammary gland transformation. Integr Biol (Cambridge). 2011; 3:910–21. [PubMed: 21842067]
29. Saxena M, Christofori G. Rebuilding cancer metastasis in the mouse. Mol Oncol. 2013; 7:283–96. [PubMed: 23474222]
30. Lifsted T, Le Voyer T, Williams M, Muller W, Klein-Szanto A, Buetow KH, et al. Identification of inbred mouse strains harboring genetic modifiers of mammary tumor age of onset and metastatic progression. Int J Cancer. 1998; 77:640–4. [PubMed: 9679770]
31. Ye XZ, Yu SC, Bian XW. Contribution of myeloid-derived suppressor cells to tumor-induced immune suppression, angiogenesis, invasion and metastasis. J Genet Genomics. 2010; 37:423–30. [PubMed: 20659706]
32. Sceneay J, Chow MT, Chen A, Halse HM, Wong CS, Andrews DM, et al. Primary tumor hypoxia recruits CD11b+/Ly6Cmed/Ly6G+ immune suppressor cells and compromises NK cell cytotoxicity in the premetastatic niche. Cancer Res. 2012; 72:3906–11. [PubMed: 22751463]
33. Hiratsuka S, Watanabe A, Aburatani H, Maru Y. Tumour-mediated upregulation of chemoattractants and recruitment of myeloid cells predetermines lung metastasis. Nat Cell Biol. 2006; 8:1369–75. [PubMed: 17128264]
34. Psaila B, Lyden D. The metastatic niche: adapting the foreign soil. Nat Rev Cancer. 2009; 9:285–93. [PubMed: 19308068]
35. Spano D, Zollo M. Tumor microenvironment: a main actor in the metastasis process. Clin Exp Metastasis. 2012; 29:381–95. [PubMed: 22322279]
36. Zhang Q, Triplett AA, Harms DW, Lin W, Creamer BA, Rizzino A, et al. Temporally and spatially controlled expression of transgenes in embryonic and adult tissues. Transgenic Res. 2010; 19:499–509. [PubMed: 19821046]
37. Borowsky A, Namba R, Young LJ, Hunter KW, Hodgson JG, Tepper CG, et al. Syngeneic mouse mammary carcinoma cell lines: two closely related cell lines with divergent metastatic behavior. Clin Exp Metastasis. 2005; 22:47–59. [PubMed: 16132578]
38. Hollern DP, Honeysett J, Cardiff RD, Andrechek ER. The E2F transcription factors regulate tumor development and metastasis in a mouse model of metastatic breast cancer. Mol Cell Biol. 2014; 34:3229–43. [PubMed: 24934442]
39. Peng L, Ran YL, Hu H, Yu L, Liu Q, Zhou Z, et al. Secreted LOXL2 is a novel therapeutic target that promotes gastric cancer metastasis via the Src/FAK pathway. Carcinogenesis. 2009; 30:1660–9. [PubMed: 19625348]
40. Moon H-J, Finney J, Xu L, Moore D, Welch DR, Mure M. MCF-7 cells expressing nuclear associated Lysyl Oxidase-like 2 (LOXL2), exhibit an Epithelial-to-Mesenchymal Transition (EMT) phenotype and are highly invasive in vitro. J Biol Chem. 2013; 288:30000–8. [PubMed: 24014025]
41. Nguyen LTT, Song YW, Nguyen SKC. Baicalein inhibits Epithelial to Mesenchymal Transition via downregulation of Cyr61 and LOXL-2 in MDA-MB231 breast cancer cells. Mol Cells. 2016; 39:909–14. [PubMed: 28008161]
42. Cheung KJ, Padmanaban V, Silvestri V, Schipper K, Cohen JD, Fairchild AN, et al. Polyclonal breast cancer metastases arise from collective dissemination of keratin 14-expressing tumor cell clusters. Proc Natl Acad Sci U S A. 2016; 113:E854–63. [PubMed: 26831077]
43. Lin EY, Jones JG, Li P, Zhu L, Whitney KD, Muller WJ, et al. Progression to malignancy in the polyoma middle T oncoprotein mouse breast cancer model provides a reliable model for human diseases. Am J Pathol. 2003; 163:2113–26. [PubMed: 14578209]

44. Herschkowitz JI, Simin K, Weigman VJ, Mikaelian I, Usary J, Hu Z, et al. Identification of conserved gene expression features between murine mammary carcinoma models and human breast tumors. Genome Biol. 2007; 8:R76. [PubMed: 17493263]
45. Kaplan RN, Riba RD, Zacharoulis S, Bramley AH, Vincent L, Costa C, et al. VEGFR1-positive haematopoietic bone marrow progenitors initiate the pre-metastatic niche. Nature. 2005; 438:820–7. [PubMed: 16341007]
46. Oskarsson T, Acharyya S, Zhang XH, Vanharanta S, Tavazoie SF, Morris PG, et al. Breast cancer cells produce tenascin C as a metastatic niche component to colonize the lungs. Nat Med. 2011; 17:867–74. [PubMed: 21706029]
47. Sinha P, Okoro C, Foell D, Freeze HH, Ostrand-Rosenberg S, Srikrishna G. Proinflammatory S100 proteins regulate the accumulation of myeloid-derived suppressor cells. J Immunol. 2008; 181:4666–75. [PubMed: 18802069]
48. Gabrilovich DI, Nagaraj S. Myeloid-derived suppressor cells as regulators of the immune system. Nat Rev Immunol. 2009; 9:162–74. [PubMed: 19197294]
49. Grossman M, Ben-Chetrit N, Zhuravlev A, Afik R, Bassat E, Solomonov I, et al. Tumor cell invasion can be blocked by modulators of collagen fibril alignment that control assembly of the extracellular matrix. Cancer Res. 2016; 76:4249–58. [PubMed: 27221706]
50. Hollosi P, Yakushiji JK, Fong KS, Csiszar K, Fong SF. Lysyl oxidase-like 2 promotes migration in noninvasive breast cancer cells but not in normal breast epithelial cells. Int J Cancer. 2009; 125:318–27. [PubMed: 19330836]
51. Tran HD, Luitel K, Kim M, Zhang K, Longmore GD, Tran DD. Transient SNAIL1 expression Is necessary for metastatic competence in breast cancer. Cancer Res. 2014; 74:6330–40. [PubMed: 25164016]
52. Weidenfeld K, Schif-Zuck S, Abu-Tayeh H, Kang K, Kessler O, Weissmann M, et al. Dormant tumor cells expressing LOXL2 acquire a stem-like phenotype mediating their transition to proliferative growth. Oncotarget. 2016; 7:71362–77. [PubMed: 27655685]
53. Chang J, Lucas MC, Leonte LE, Garcia-Montolio M, Singh LB, Findlay AD, et al. Pre-clinical evaluation of small molecule LOXL2 inhibitors in breast cancer. Oncotarget. 2017; 18:26066–78.

Europe PMC Funders Author Manuscripts

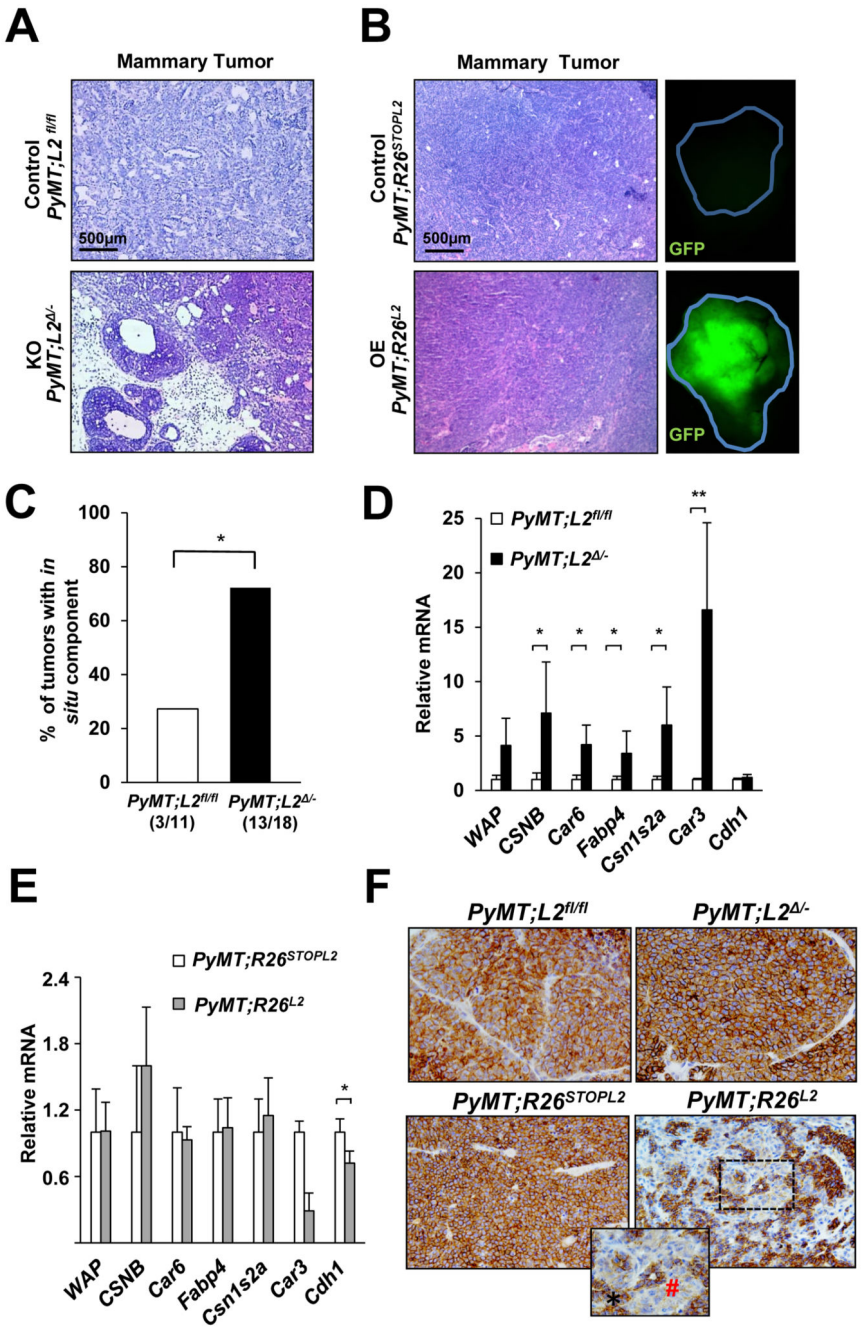

Figure 1. Loxl2 promotes PyMT tumor epithelial dedifferentiation and local invasion.

(**A, B**) Representative H&E images of paraffin-embedded tumors from *PyMT;L2*$^{\Delta/-}$ and *PyMT;R26*^{L2} 16 week-old mice and their respective controls. In the case of the overexpression model (**B**), representative GFP images of primary tumors are also shown (right panels). Scale bars: 500 μm. (**C**) Percentage of primary breast tumors containing regions of in situ carcinoma developed by *PyMT;Loxl2*$^{fl/fl}$ and PyMT;L2$^{\Delta/-}$ mice. The number of tumors with *in situ* component over the total number of analyzed tumors from reach genotype is shown in the bottom; *P< 0.05 (Fisher's exact test). (**D, E**) Primary

tumors of 14 week-old *PyMT;R26*^{L2} (**D**) and *PyMT;L2*$^{\Delta/-}$ (**E**) mice and their paired controls (n=5, each) were subjected to RT-qPCR analyses for the indicated differentiation markers. Error bars represent standard error. *P<0.05; **0.001<P<0.005 (Student's t-test; unpaired, 2-tailed). (**F**) Representative E-cadherin immunohistochemical images in PyMT tumors with modified Loxl2 expression: *PyMT;L2*$^{\Delta/-}$ (upper right) and *PyMT;R26*^{L2} (bottom right) as well as in their specific controls *PyMT;L2*$^{fl/fl}$ (upper left) and *PyMT;R26*^{STOPL2} (bottom left), respectively; x20 magnification. Inset shows a specific heterogeneous staining area with conserved (*, black) and reduced (#, red) E-cadherin in one representative *PyMT;R26*^{L2} tumor; x40 magnification.

Europe PMC Funders Author Manuscripts

Europe PMC Funders Author Manuscripts

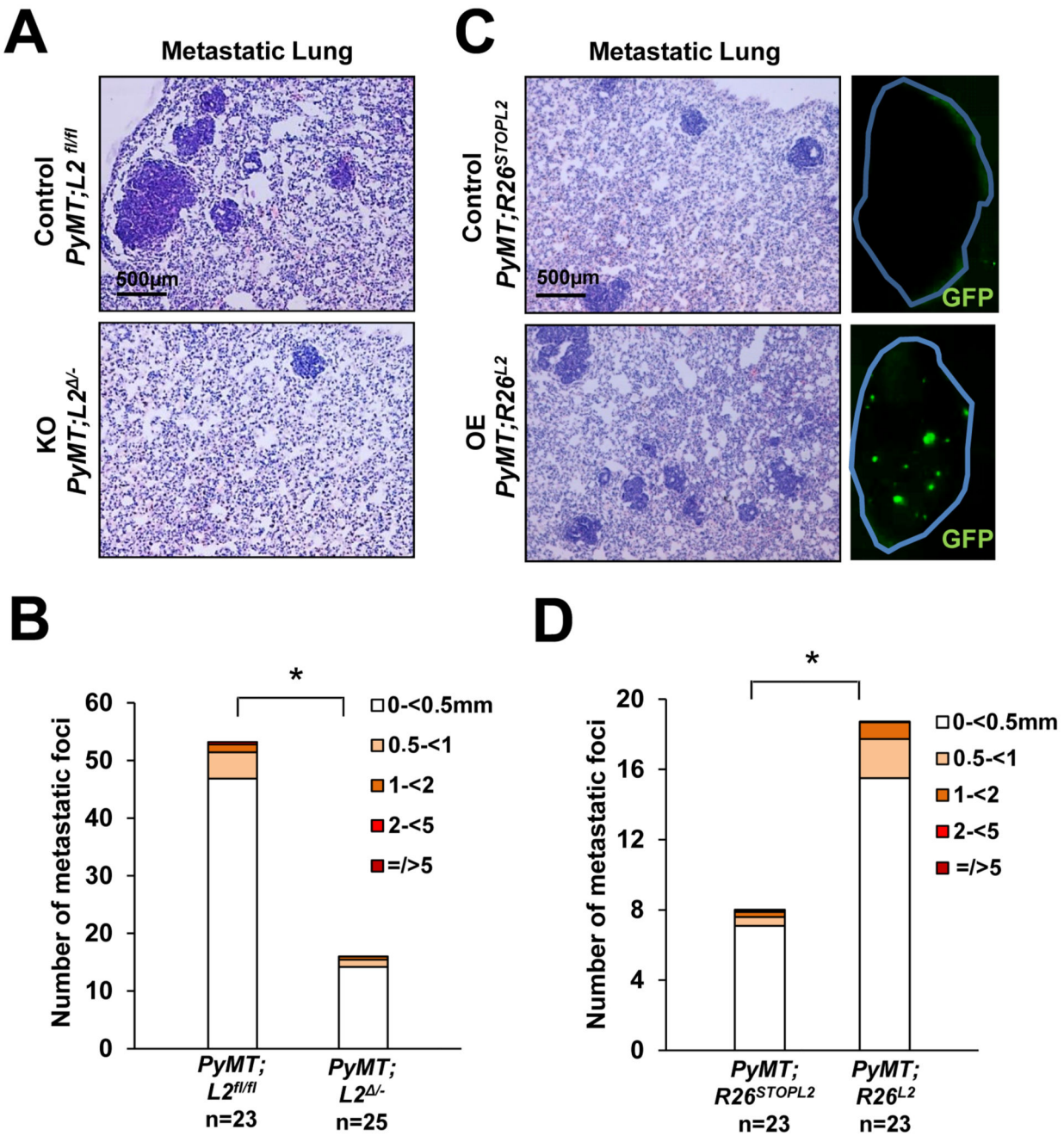

Figure 2. Loxl2 enhances PyMT lung metastatic burden.

(**A, C**) Representative H&E stained lung sections from *PyMT;L2*$^{\Delta/-}$ (**A**) and *PyMT;R26*^{L2} (**C**) 16 week-old mice and their corresponding tumor bearing controls. GFP images of metastatic lungs from the overexpression Loxl2 model are also shown in C (right panels). Scale bars: 500 μm. (**B, D**) Quantification of average number and size of lung metastatic foci developed by *PyMT;L2*$^{\Delta/-}$ (**B**) and *PyMT;R26*^{L2} (**D**) mice at 16 weeks of age and their paired controls. The number of analyzed mice from each genotype is shown at the bottom

and size of lesions by color code. Error bars represent standard error. *P<0.05 (Student's t-test; unpaired, 2-tailed).

Europe PMC Funders Author Manuscripts

Europe PMC Funders Author Manuscripts

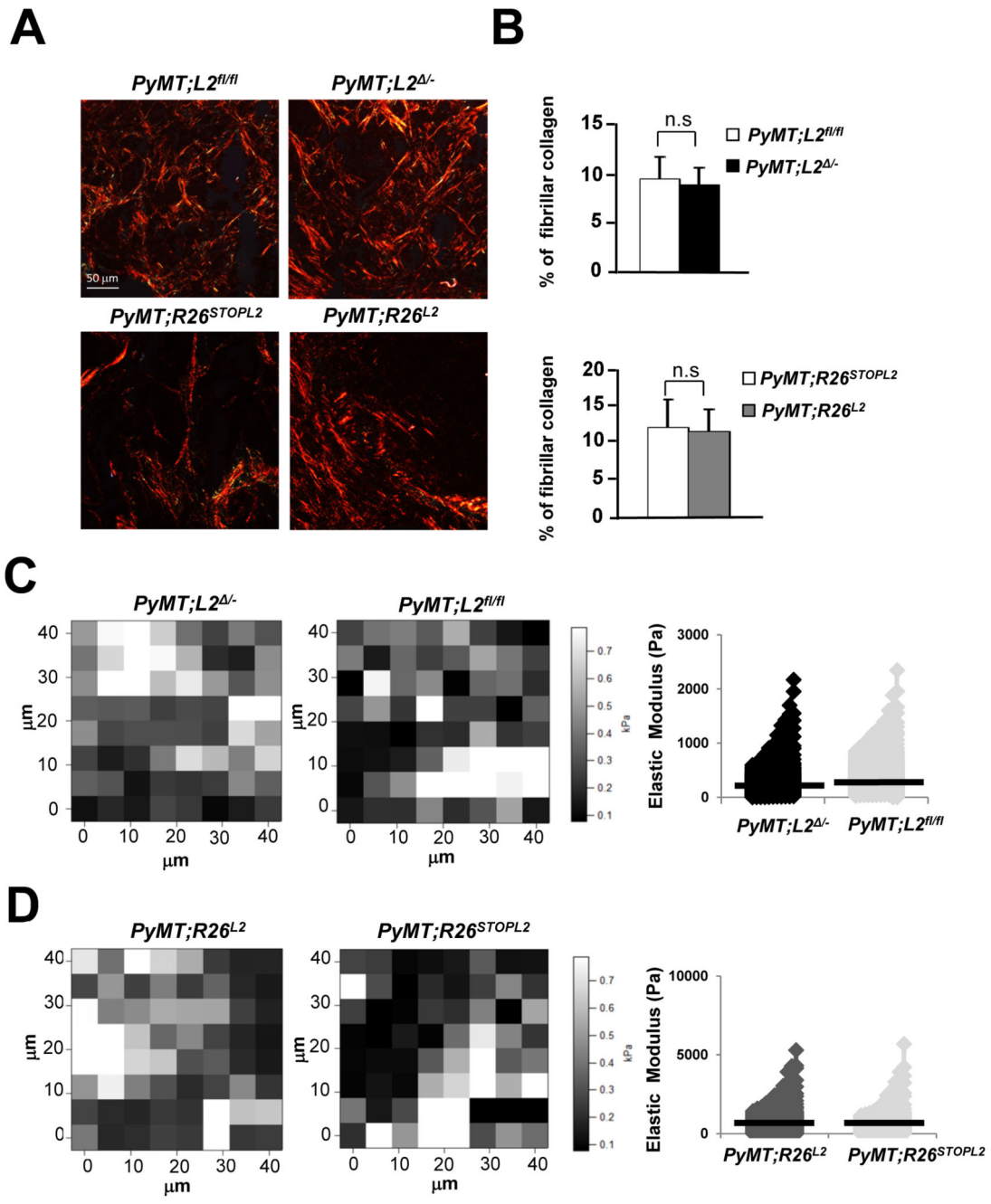

Figure 3. Aberrant expression of Loxl2 does not affect collagen ECM stiffness of PyMT primary tumors.

(**A**) Representative images of picrosirius-red staining of PyMT tumors lacking (upper) and overexpressing Loxl2 (bottom) compared with their respective controls. Scale bars: 50 μm. (**B**) Quantification of threshold pixel density representing positive picrosirius staining for tumors of the indicated genotypes. Error bars represent standard error, n.s. not statistically significant. (**C, D**) Atomic force microscopy (AFM) analysis of PyMT primary tumors. Left, representative forcemaps (40 μm x 40 μm) depicting typical elastic modulus values of

stroma-rich regions of the tumors of the indicated genotypes. Right, quantitative analysis of AFM microscopy data showing similar values in all PyMT tumors regardless Loxl2 expression. Bars represent average elastic modulus for control *PyMT;L2*$^{fl/fl}$ (black, 353.17 Pa), *PyMT;L2*$^{\Delta/-}$ (light grey, 260.78 Pa), control *PyMT;R26*^{STOPL2} (dark grey, 401.50 Pa) and *PyMT;R26*^{L2} (light grey, 418.77 Pa) mouse groups. Data represent 4 mice from each condition, with 2 tissue sections from each mouse, and measurements taken from at least 5 different locations on each tissue section.

Europe PMC Funders Author Manuscripts

Europe PMC Funders Author Manuscripts

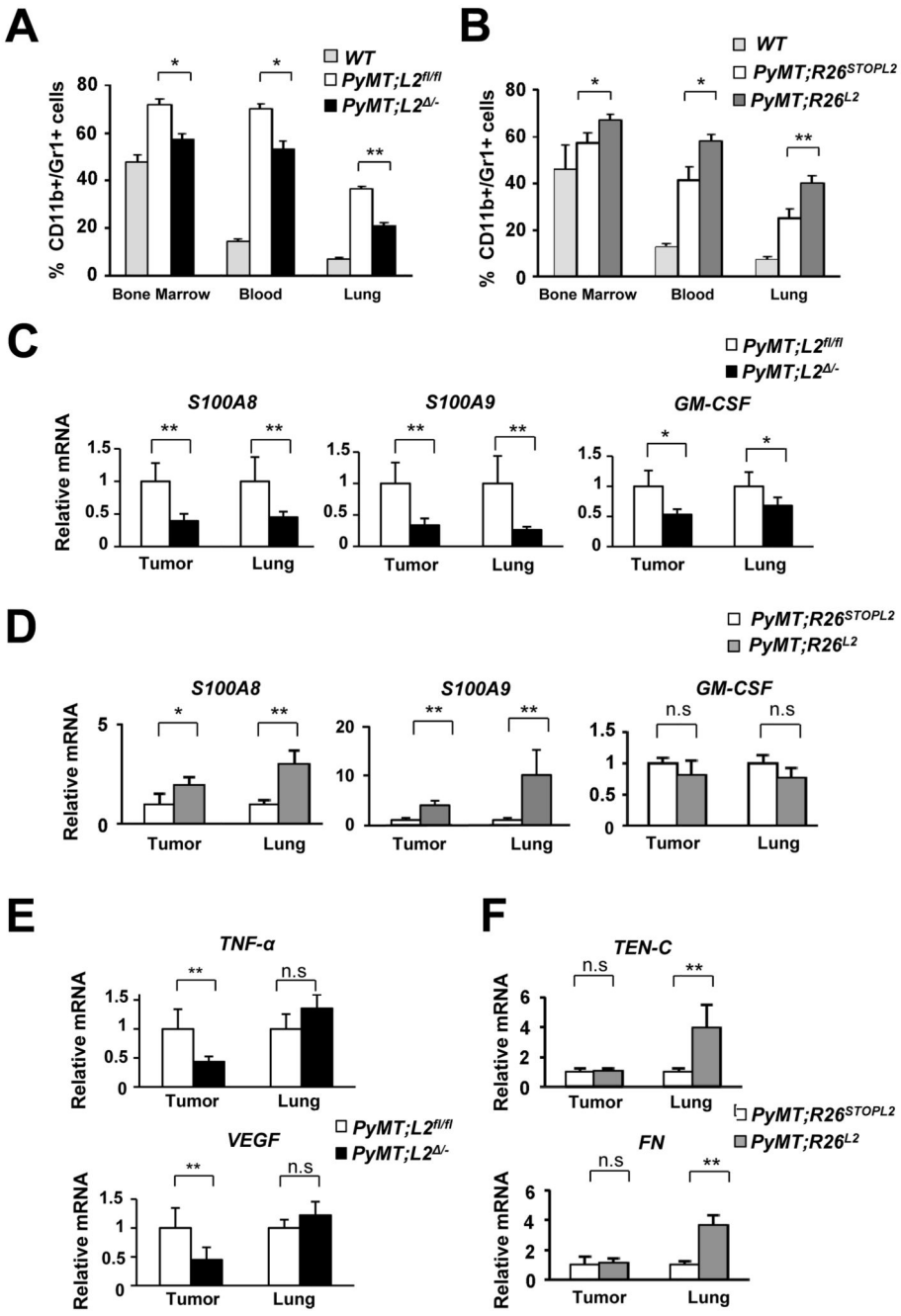

Figure 4. Loxl2 positively modulates CD11b+/Gr1+ cell recruitment and cytokine production.

(**A, B**) Content of CD11b+/Gr1+ double positive cells in bone marrow, blood and lung samples from wt, *PyMT;L2*$^{fl/fl}$, *PyMT; L2*$^{\Delta/-}$ (**A**) and wt, *PyMT;R26*^{STOPL2} and *PyMT;R26*^{L2} (**B**) 14 week-old mice, determined by FACs analysis. Tissue samples analyzed: 7 pools of two mice per tissue for *PyMT;L2*$^{fl/fl}$ and *PyMT;L2*$^{\Delta/-}$ mouse cohorts; 6 *PyMT;R26*^{STOPL2} and 8 *PyMT;R26*^{L2} mice, and 2 pools for the tumor-free animals (wt). (**C, D**) Quantitative RT-qPCR analyses of *S100A8*, *S100A9* and *GM-CSF* in tumors and lungs from (**C**) *PyMT;L2*$^{fl/fl}$ and *PyMT;L2*$^{\Delta/-}$, and (**D**) *PyMT;R26*^{STOPL2} and *PyMT;R26*^{L2} 14

week-old mice. (**E**) Quantification of *TNF-a* and *VEGF* expression levels by RT-qPCR in primary tumors and lungs of the indicated genotypes. (**F**) RT-qPCR analysis of tenascin-C (*Ten-C*) and fibronectin (*FN*) mRNA levels in primary tumors and lungs of the indicated genotypes. RNA from 5 primary tumors and 4 lung samples per genotype was used in all the assays. Bars represent standard error. *P< 0.05; **0.001<P< 0.005; n.s. not significant (Student's *t*-test; unpaired, 2-tailed).

Europe PMC Funders Author Manuscripts

Europe PMC Funders Author Manuscripts

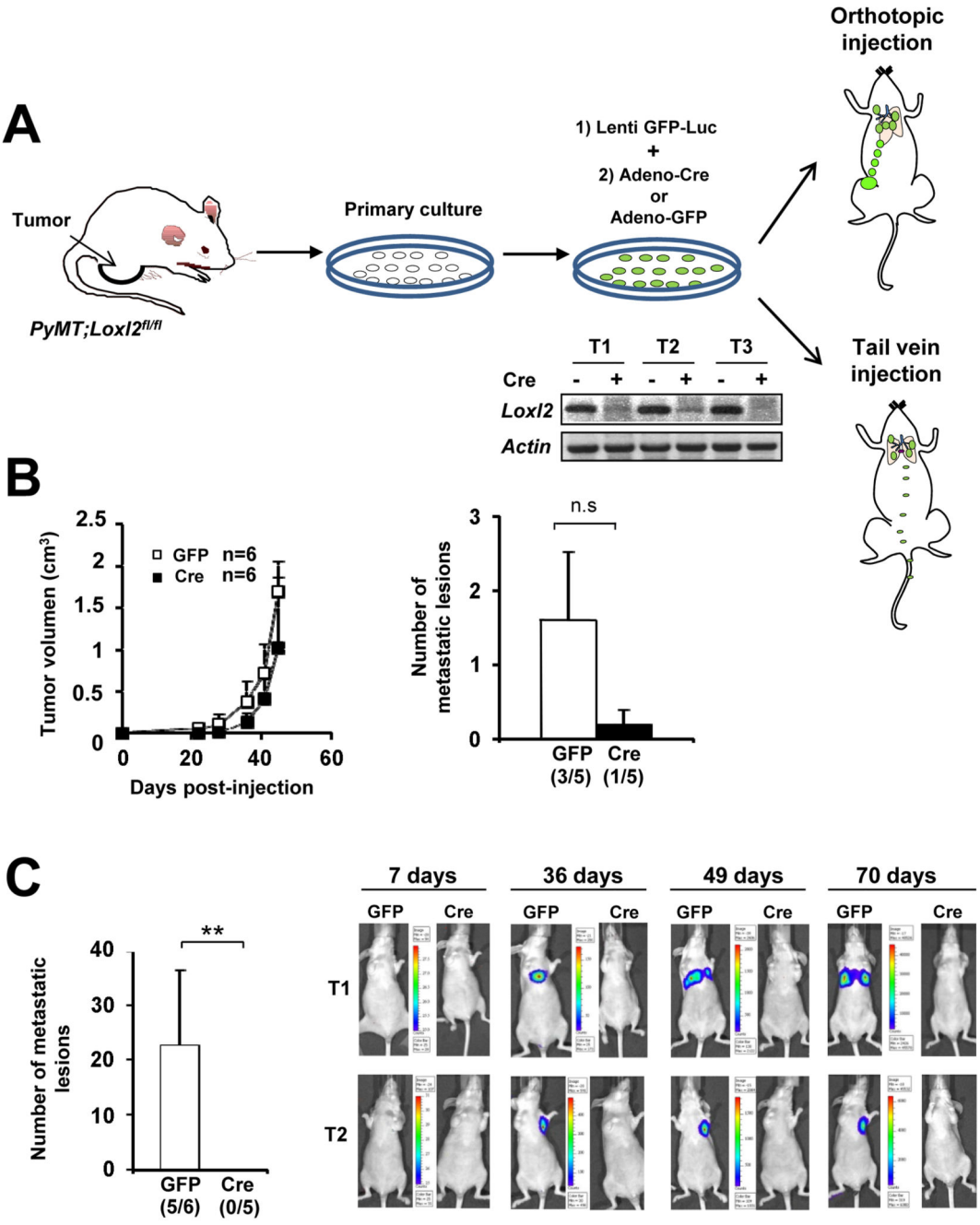

Figure 5. ***In vitro*** **abrogation of Loxl2 critically diminishes the metastatic capacity of PyMT mammary tumor cells.**

(**A**) Diagram representing the strategy followed for isolation and generation of PyMT cells used in the indicated tumorigenesis assays. Primary breast cancer cells were isolated from mammary tumors developed by control *PyMT; L2*$^{fl/fl}$ mice and grown in culture. Cells were first lentivirally infected with a GFP-Luciferase vector, and then transduced with control GFP- or Cre-adenovirus. *Loxl2* depletion in cell lines from three independent PyMT tumors was confirmed by semi-quantitative RT-PCR (middle, bottom). Deleted and control Loxl2

cells were orthotopically inoculated in the mammary fat pad (right, upper) or tail vein injected (lower) into nude mice. (**B**) Quantification of tumor size (left) and metastatic foci (right) after orthotopic injection of both control and Loxl2 depleted primary PyMT cell lines; the number of mice with metastasis is indicated below the graphs. Error bars represent standard error. n.s., not significant (Student's *t*-test; unpaired, 2-tailed). (**C**) Left, number of lung metastasis foci from tail vein injected mice with adeno-GFP or adeno-Cre cells; the number of mice with metastasis is indicated below the graphs. Error bars represent standard error. **0.001<*P*<0.005; n.s., not significant (Student's *t*-test; unpaired, 2-tailed). Right, representative bioluminescence images of intravenously injected mice with control adeno-GFP or adeno-Cre cells isolated from two independent PyMT tumors. Images were obtained at the indicated days after tail vein injection. The color scale represents the photon flux (photons per second) emitted from the lung region of xenografted mice. All the experiments were performed in duplicates with stable cell cultures derived from three different PyMT tumors (T1-T3).

Europe PMC Funders Author Manuscripts

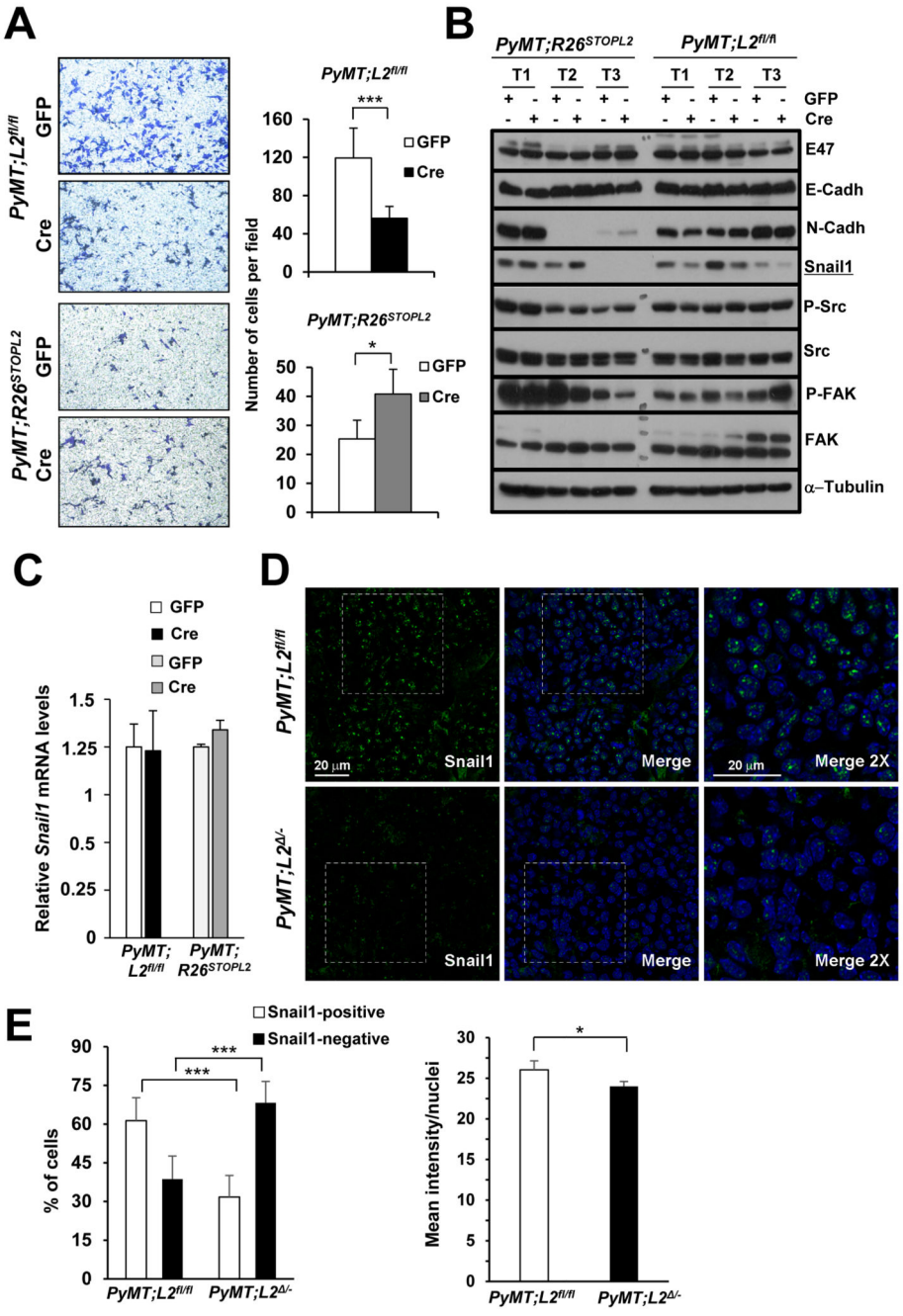

Figure 6. Loxl2 modulates invasiveness of PyMT cells and Snail1 protein levels.

(**A**) Representative images of invasion assays on matrigel (left panels) and quantification (right panels) of PyMT cells (n=3, each) displaying altered levels of Loxl2 as indicated. Error bars represent standard error. **P*<0.05; ****P*<0.001 (Student's *t*-test; unpaired, 2-tailed). (**B**) Protein levels of different EMT and migration markers in three independent PyMT cell lines (T1, T2, T3) generated from the indicated genotypes infected or not with Cre recombinase; α-tubulin was used as loading control. (**C**) Quantification of *Snail1* mRNA levels by RT-qPCR in PyMT cells with Loxl2 deletion or overexpression and

corresponding controls in one representative cell culture of each of the genotypes. (**D**) Representative images of immunofluorescence analysis of Snail1 expression (green) in PyMT tumors lacking Loxl2 (bottom panels) compared with their paired controls (upper panels) revealing decreased nuclear Snail1 levels in the absence of Loxl2. Nuclei are detected with Dapi (blue). Merge confocal microscopy images (middle panels) and magnifications (x2) are shown (right panels). Scale bar: 20 μm. (**E**) Quantitation of the percentage Snail1-positive and Snail1-negative cells (left) and the mean intensity of Snail1 nuclear staining (arbitrary units) (right). A minimum of three random fields were analyzed per sample (n=6 for *PyMT;L2*$^{fl/fl}$; n=7 for *PyMT;L2*$^{\Delta/-}$). Error bars represent standard error. *P<0.05; ***P<0.001 (Student's *t*-test; unpaired, 2-tailed).

Europe PMC Funders Author Manuscripts

Europe PMC Funders Author Manuscripts

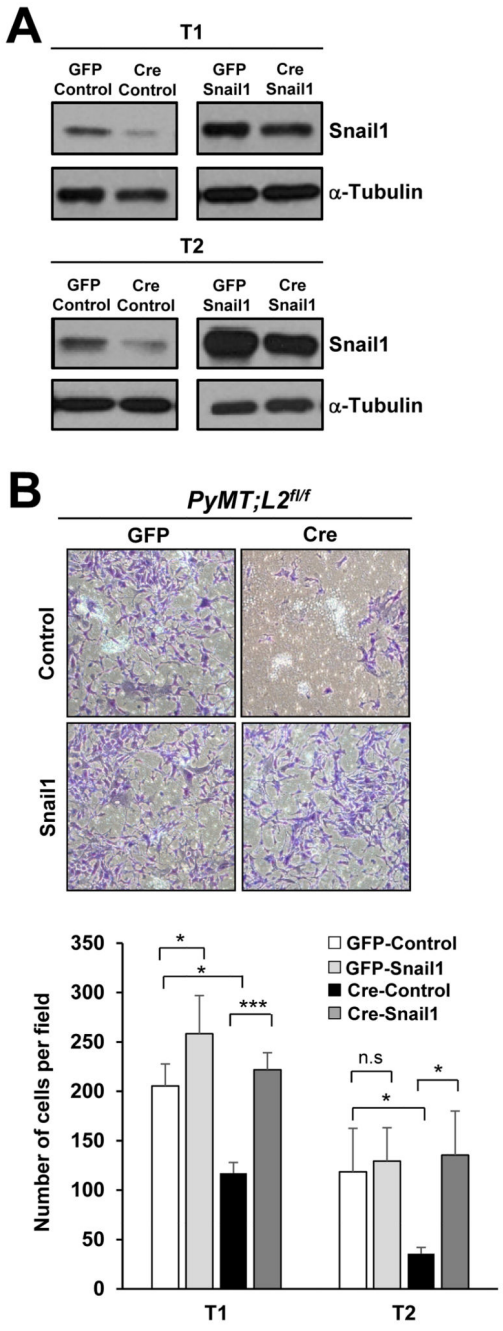

Figure 7. Snail1 overexpression restores invasive properties of PyMT-Loxl2 deficient cells.

(**A**) Snail1 protein levels of PyMT-GFP (control) and PyMT-Cre (Loxl2-deficient) cell lines *in vitro* manipulated for Snail1 overexpression (GFP-Snail1 and Cre-Snail1) (right panels) or empty control vector (left panels) by lentiviral infection. α-tubulin was used as loading control. (**B**) Representative images of invasion assays on matrigel (upper panels) and quantification (bottom panel) of *PyMT;L2*$^{fl/fl}$-GFP and *PyMT;L2*$^{fl/fl}$-Cre cells overexpressing Snail1 or control vector. Experiments were performed twice with two independent PyMT tumor cell lines (T1, T2); triplicates for each of the Loxl2 and Snail1

combinations were analyzed. Error bars represent standard error. *P<0.05; ***P< 0.001; n.s., not significant (Student's t-test; unpaired, 2-tailed).

Europe PMC Funders Author Manuscripts